Liquid Crystals
Publication details, including instructions for authors and subscription information:
http://www.informaworld.com/smpp/title~content=t713926090

Phase behaviour of three homologues of the discotic hexa-*n*-alkoxyanthraquinones under pressure

Yoji Maeda[a]; Hiroshi Yokoyama[a]; Sandeep Kumar[b]
[a] Nanotechnology Research Institute, National Institute of Advanced Industrial Science and Technology, Tsukuba, Ibaraki 305-8565, Japan [b] Raman Research Institute, Bangalore 560 080, India

To cite this Article Maeda, Yoji , Yokoyama, Hiroshi and Kumar, Sandeep(2005) 'Phase behaviour of three homologues of the discotic hexa-*n*-alkoxyanthraquinones under pressure', Liquid Crystals, 32: 7, 833 — 845
To link to this Article: DOI: 10.1080/02678290500228055
URL: http://dx.doi.org/10.1080/02678290500228055

Liquid Crystals, Vol. 32, No. 7, July 2005, 833–845

Phase behaviour of three homologues of the discotic hexa-*n*-alkoxyanthraquinones under pressure

YOJI MAEDA*†, HIROSHI YOKOYAMA† and SANDEEP KUMAR‡

†Nanotechnology Research Institute, National Institute of Advanced Industrial Science and Technology, Higashi 1-1-1, Tsukuba, Ibaraki 305-8565, Japan

‡Raman Research Institute, C. V. Raman Avenue, Bangalore 560 080, India

(*Received 14 March 2005; accepted 12 April 2005*)

The phase transition behaviour of three homologous discotic mesogens, the hexa-*n*-alkoxyanthraquinones HOAQ(*n*), *n* indicating the number of carbon atoms in the alkoxy group, was investigated under hydrostatic pressures up to 500 MPa using a high pressure differential thermal analyser. The *T* vs. *P* phase diagrams of HOAQ(6), HOAQ(8) and HOAQ(9) were constructed for solution- (Cr_0) and melt-crystallized (Cr_1) samples of the compounds. HOAQ(6) shows the reversible Cr_0–rectangular columnar phase (Col_r) –hexagonal columnar phase (Col_h)–isotropic liquid (I) phase sequence at atmospheric pressure. The stable Col_r phase of HOAQ(6) has a decreased temperature range with increasing pressure and then the Col_r phase disappears under pressures above about 350 MPa; instead the Cr_0–Col_h–I phase sequence is exhibited. For HOAQ(8), the solution-grown sample exhibits the stable Cr_0–Col_h–I phase sequence at atmospheric pressure. Applying pressure to the solution-grown sample induces the formation of the stable Col_r phase in the pressure region between 10 and 350 MPa, leading to the Cr_0–Col_r–Col_h–I phase sequence. The pressure-induced Col_r phase disappears under higher pressures. The melt-cooled sample of HOAQ(8) shows the formation of the metastable crystal (Cr_1), unknown mesophase (X) and Col_r phases at lower temperatures under atmospheric pressure, and exhibits the reversible Cr_1–X–Col_r–Col_h–I phase sequence on subsequent thermal cycles. The metastable phase sequence was observed under pressures up to 100 MPa, but the phase transitions were too small to be detected under higher pressures. In HOAQ(9) the stable Cr_0–Col_h–I phase sequence is observed at all pressures, while the melt-cooled sample shows the metastable Cr_1–Col_r–Col_h–I phase sequence under pressures up to 300 MPa. The metastable Col_r phase disappears under higher pressures.

1. Introduction

In 1977 it was first shown that disc-shaped molecules consisting of a rigid aromatic core and a number of flexible aliphatic side chains form stable mesophases in which the discs are stacked on top of each other to form columns [1]. Since the discovery of discotic liquid crystals, a number of papers have appeared on the synthesis and characterization of novel disc-like mesogens which have been reported to form columnar mesophases [2–7]. Four different columnar mesophases have been identified, the difference being attributed to the regular or irregular stacking of discs along the columns, packed either in hexagonal or rectangular arrangements [2]. The structural peculiarity of this class of mesogens is the presence of a molecular skeleton consisting of a flat disc-like part connected to either six or eight flexible chains. Among these, anthraquinone (rufigallol) derivatives are one of the earliest systems known to form such types of mesophase [8–10]. In the anthraquinone derivatives reported so far, the flexible part consists of normal aliphatic chains bound to the central core by ether or ester linkages. The 1,2,3,5,6,7-hexa-*n*-alkoxyanthraquinones, abbreviated here as HOAQ(*n*), *n* indicating the number of carbon atoms in the alkoxy group, are typical examples of such discotic mesogens. The chemical structure of HOAQ(*n*) is:

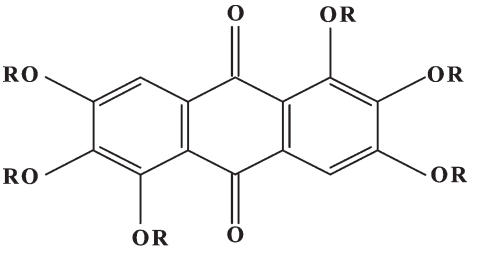

R = C_nH_{2n+1} (*n*= 6, 8, 9)

*Corresponding author. Email: yoji.maeda@aist.go.jp

Liquid Crystals
ISSN 0267-8292 print/ISSN 1366-5855 online © 2005 Taylor & Francis
http://www.tandf.co.uk/journals
DOI: 10.1080/02678290500228055

The thermal properties of the HOAQ(n) homologous series have been reported by Carfagna *et al.* [9], and these included a multiplicity of solid phases stable at different temperatures and with different crystal structures between solution- and melt-crystallized samples. The transition temperature to the isotropic liquid decreases smoothly with increasing length of the chains, indicating that the stability of the columnar mesophase is related to the length of the flexible alkyl chains. The X-ray diffraction patterns of the mesophases support their discotic structure with the hexagonal packing of the columns. On cooling the normal columnar phase, a highly ordered phase is often formed for these derivatives [11, 12]. Similar highly ordered phases exhibited by triphenylene derivatives have been characterized as discotic plastic and helical phases [13–15].

We have previously reported the phase behaviour of two discotic mesogens, viz. 5,10,15,20-tetrakis(4-*n*-dodecylphenyl)porphyrin (C12TPP) [16, 17] and 2,3,6,7,10,11-hexahexylthiotriphenylene (HHTT) [18], under hydrostatic pressure using a high pressure differential thermal analyser (DTA) and a wide angle X-ray diffractometer equipped with a high pressure system. C12TPP showed the discotic lamellar phase (D_L) between the crystal and isotropic liquid, in which the phase stability of the D_L phase decreased with increasing pressure up to about 200 MPa. The T–P phase diagram of the sample cooled at 300 MPa clearly showed a triple point for the pressure-crystallized solid, D_L, and isotropic liquid phases at about 241 MPa, indicating the upper limit of pressure for the formation of the D_L phase. HHTT is a well known substance with high mobility of charge carrier in the mesophase, two or three orders of magnitude higher than those in the normal columnar phase [19, 20]. The enantiotropic phase transitions of HHTT, i.e. crystal (Cr)–helical phase (H), H–hexagonal columnar phase (Col_h), and Col_h–I transitions, are held at pressures up to 32 MPa. The application of pressures above 32 MPa transformed the H and Col_h phases into monotropic phases, depending upon the applied pressure. The helical phase was observed as a monotropic phase in the pressure region between 32 and about 180 MPa. Thus the I–Col_h–H–Cr transition sequence appeared on cooling under pressures, while the Cr–Col_h–I sequence occurred on subsequent heating. Further increases in pressure above 200 MPa changed the enantiotropic Col_h phase into a monotropic phase. Thus the I–Col_h–Cr phase sequence appeared on cooling at higher pressures, while the Cr–I transition was observed on subsequent heating. The T–P phase diagram of HHTT obtained in the heating mode possessed two triple points: one was for the H phase and another for the Col_h phase, indicating the upper limits of pressure for the H and Col_h phases, respectively. Such interesting phase behaviour of C12TPP and HHTT under hydrostatic pressure prompted us to study the phase behaviour of HOAQ(n) mesogens with different alkoxy chains under pressure, particularly focused on the effect of pressure on the stability of the normal columnar and highly ordered columnar phases.

In this paper, we present the experimental results of the thermal behaviour of three homologues belonging to the hexa-*n*-alkoxyanthraquinone series HOAQ(n) with hexyloxy (n=6), octyloxy (n=8) and nonyloxy (n=9) groups under hydrostatic pressures up to 500 MPa using a high pressure DTA.

2. Experimental

2.1. *Sample characterization at ambient pressure*

Discotic liquid crystalline derivatives of anthraquinone HOAQ(6), HOAQ(8) and HOAQ(9) were prepared from rufigallol (1,2,3,5,6,7-hexahydroxyanthra-9,10-quinone). Acid-catalysed self-condensation of gallic acid yields crude rufigallol which was purified through its hexaacetate [21]. Alkylation of the rufigallol hexaacetate with the appropriate alkyl bromide yields the desired hexa-*n*-alkoxyanthraquinone. In a typical procedure, 1 mmol of rufigallol hexaacetate was dissolved in 5 ml of *N*,*N*′-dimethylformamide with 12 mmol of sodium carbonate and 15 mmol of the appropriate alkyl bromide. The mixture was heated at 160°C under nitrogen. The cooled reaction mixture was poured into ice-water and the resultant precipitate filtered off. The dried crude product was purified by column chromatography over silica gel followed by crystallization from a mixture of hexane, acetone and methanol or hexane, ether and ethanol. The purity of the product was checked by TLC, IR and ^{1}H NMR.

Thermal characterization was performed on a Perkin-Elmer Pyris-1 differential scanning calorimeter (DSC) at a scanning rate of 5°C min^{-1} under N_2 gas flow. Temperatures and heats of transition were calibrated using indium and tin standards. Transition temperatures were determined as the onset of the transition peaks at which the tangential line of the inflection point of the rising part of the peak crosses over the extrapolated baseline. Morphological observation was performed using a Leiz Orthoplan polarizing optical microscope (POM) equipped with a Linkam hot stage THMS-600.

Structural characterization of the crystals and the columnar phases of HOAQ(6), HOAQ(8) and HOAQ(9) was performed using a wide angle X-ray diffractometer equipped with a hot stage (Mettler FP

82, Mettler Toledo Co. Ltd.). The sample was placed in a Lindemann-type capillary tube of 1 mm diameter, and measured using a 1.5 kW X-ray generator (R-AXIS IV, Rigaku Co.). A CuK_α X-ray beam was used to irradiate the sample and the diffraction patterns were taken using the attached imaging plate detector.

2.2. *DTA measurements under pressure*

The high pressure DTA apparatus used in this study is described elsewhere [22]. The DTA system was operated in a temperature region between room temperature and 250°C under hydrostatic pressures up to 500 MPa. Dimethylsilicone oil with a low viscosity (10 cSt) was used as the pressurizing medium. The sample was placed in the platinum DTA cell and coated with epoxy adhesives, to fix it in the bottom of the cell and also to prevent direct contact with the silicone oil. The DTA runs were performed at a constant heating rate of 5°C min^{-1} under various pressures. Peak temperatures were taken as transition temperatures for constructing the real temperature vs. pressure phase diagram.

3. Results and discussion

3.1. *Characterization at atmospheric pressure*

Figures 1, 2 and 3 show the DSC traces of the solution-grown and melt-cooled samples of HOAQ(6), HOAQ(8) and HOAQ(9) at a constant scanning rate of 5°C min^{-1}, respectively. These compounds show a hexagonal columnar (Col_h) phase between the crystalline and isotropic liquid phases [5–9]. The solution-grown and melt-cooled crystals are denoted here as Cr_0 and Cr_1, respectively. As shown in figure 1, HOAQ(6) shows reversibly melting, a mesophase transition at an intermediate temperature and isotropization. The intermediate temperature peak indicates the mesophase transition between the highly ordered rectangular columnar (Col_r) and Col_h phases [11, 12]. HOAQ(6) exhibits the reversible Cr_0–Col_r–Col_h–I phase sequence. In HOAQ(8) and HOAQ(9), on the other hand, the solution-grown samples exhibit a very large melting peak at a relatively high temperature and an

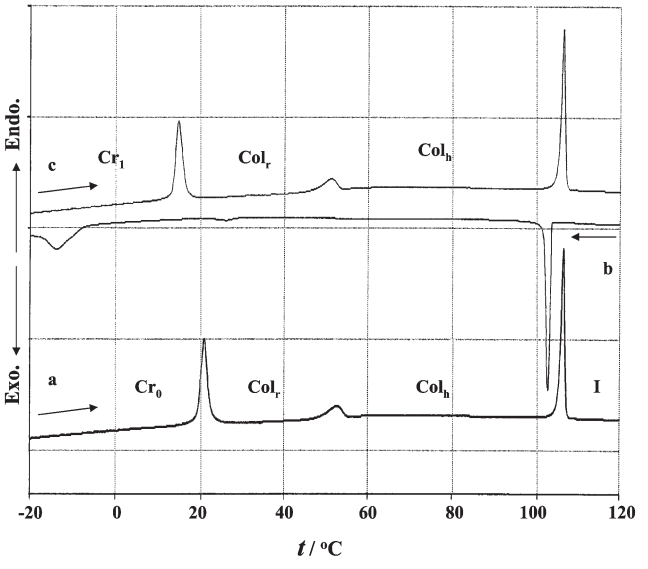

Figure 1. DSC traces of (*a*) solution- and (*b*, *c*) melt-cooled samples of HOAQ(6), Scanning rate: 5°C min^{-1}.

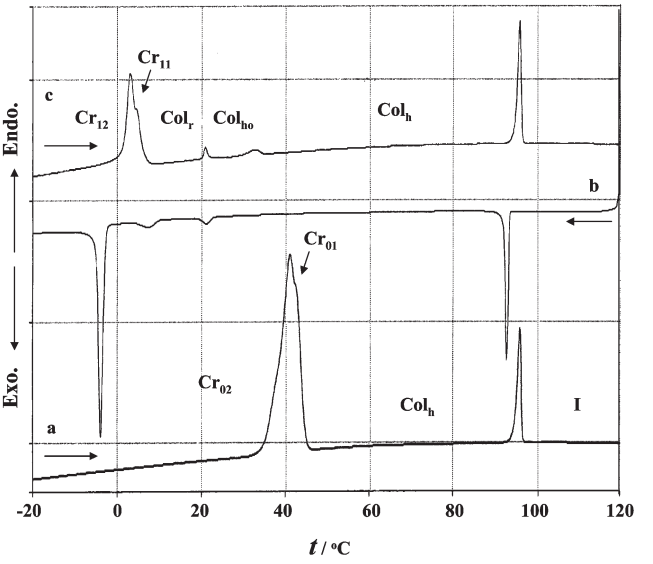

Figure 2. DSC traces of (*a*) solution- and (*b*, *c*) melt-cooled samples of HOAQ(8). Scanning rate: 5°C min^{-1}.

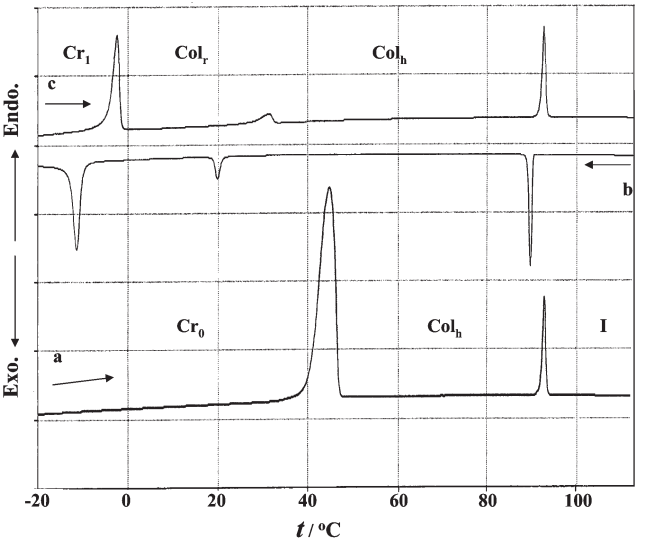

Figure 3. DSC traces of (*a*) solution- and (*b*, *c*) melt-cooled samples of HOAQ(9). Scanning rate: 5°C min^{-1}.

Table 1. Thermodynamic quantities associated with the phase transitions for HOAQ(6), HOAQ(8) and HOAQ(9).

	T/°C	ΔH/kJ mol^{-1}	ΔS/ J K^{-1} mol^{-1}
HOAQ(6)			
1st heating			
Cr_0–Col_r	19.6	11.17	38.15
Col_r–Col_h	48.5	2.81	8.73
Col_h–I	105.5	11.98	31.64
2nd heating			
Cr_1–Col_r	13.5	9.86	34.40
Col_r–Col_h	47.1	2.72	8.51
Col_h–I	105.3	11.74	31.04
HOAQ(8)			
1st heating			
Cr_0–Col_h	37.2	88.35	284.66
Col_h–I	94.8	11.72	31.85
2nd heating			
Cr_1–X	0.0	24.25	88.76
X–Col_r	20.0	1.20	4.09
Col_r–Col_h	29.8	1.45	4.80
Col_h–I	94.8	11.60	31.52
HOAQ(9)			
1st heating			
Cr_0–Col_h	40.5	109.97	350.53
Col_h–I	92.2	11.47	31.39
2nd heating			
Cr_1–Col_r	−4.4	23.36	86.92
Col_r–Col_h	27.8	3.31	10.99
Col_h–I	91.8	11.09	30.39

isotropization peak on the first heating run. The melting of the solution-grown samples in figures 2 and 3 is composed of two or three overlapped peaks, which indicate two or three crystalline polymorphs [9]. Thus HOAQ(8) and HOAQ(9) show the irreversible transition sequence of (Cr_{03})–Cr_{02}–Cr_{01}–Col_h–I on first heating. The subsequent cooling and reheating runs exhibit an additional peak of the weak Col_r–Col_h transition at a lower temperature, indicating the formation of the metastable crystalline Cr_1 and the Col_r phases. The Cr_1–Col_r–Col_h–I phase sequence of HOAQ(8) and HOAQ(9) on repeated thermal cycles is the same as for HOAQ(6). Thus the thermal behaviour indicates that the Cr_0, Col_r and Col_h phases of HOAQ(6) are thermodynamically stable, while the melt-cooled Cr_1 and Col_r phases of HOAQ(8) and HOAQ(9) are metastable, as these transition temperatures are lower than the melting point of the Cr_0

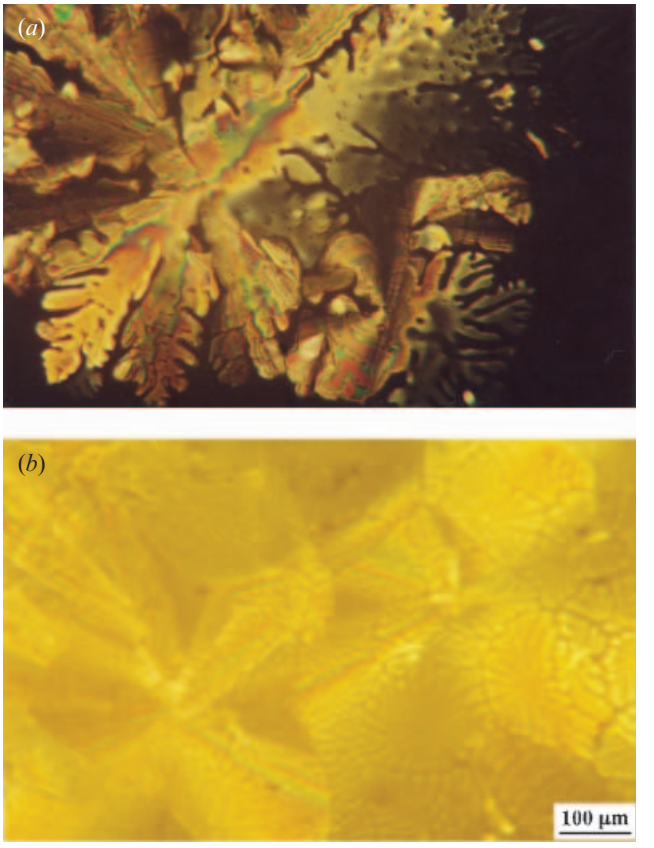

Figure 4. A flower-like texture of the Col_h phase of HOAQ(6) at (*a*) 105°C and (*b*) 80°C observed on cooling.

crystals. In HOAQ(8), furthermore, an unknown transition is observed between the Cr_1 and Col_r phases, and the Cr_1–X–Col_r–Col_h–I phase sequence is seen on subsequent thermal cycles. The Cr_1–Col_r–Col_h–I phase sequence for the HOAQ(*n*) homologues is generally seen on the repeated thermal cycles at atmospheric pressure. The thermodynamic quantities of the phase transitions of the three homologues are listed in table 1.

Figure 4 shows POM photographs of the Col_h phase of HOAQ(6) observed at 105 and 80°C on cooling from the isotropic liquid. The flower-like texture of the Col_h phase in figure 4 (*a*) is the same as previously reported by Carfagna *et al.* [9]. It is interesting to note that the flower-like texture of the Col_h phase usually changes to the typical mosaic texture with smooth surfaces on cooling, but sometimes a condensed-flower-like texture, figure 4 (*b*), was observed at lower temperatures. Figure 5 shows the changes in texture seen for HOAQ(6) on cooling from the isotropic liquid. The flower-like texture of the Col_h phase, figures 5 (*a*) and 5 (*b*), was altered to a mosaic texture with smooth surfaces and exhibiting large domains, figure 5 (*c*). Then the mosaic domains of the Col_h phase split into smaller

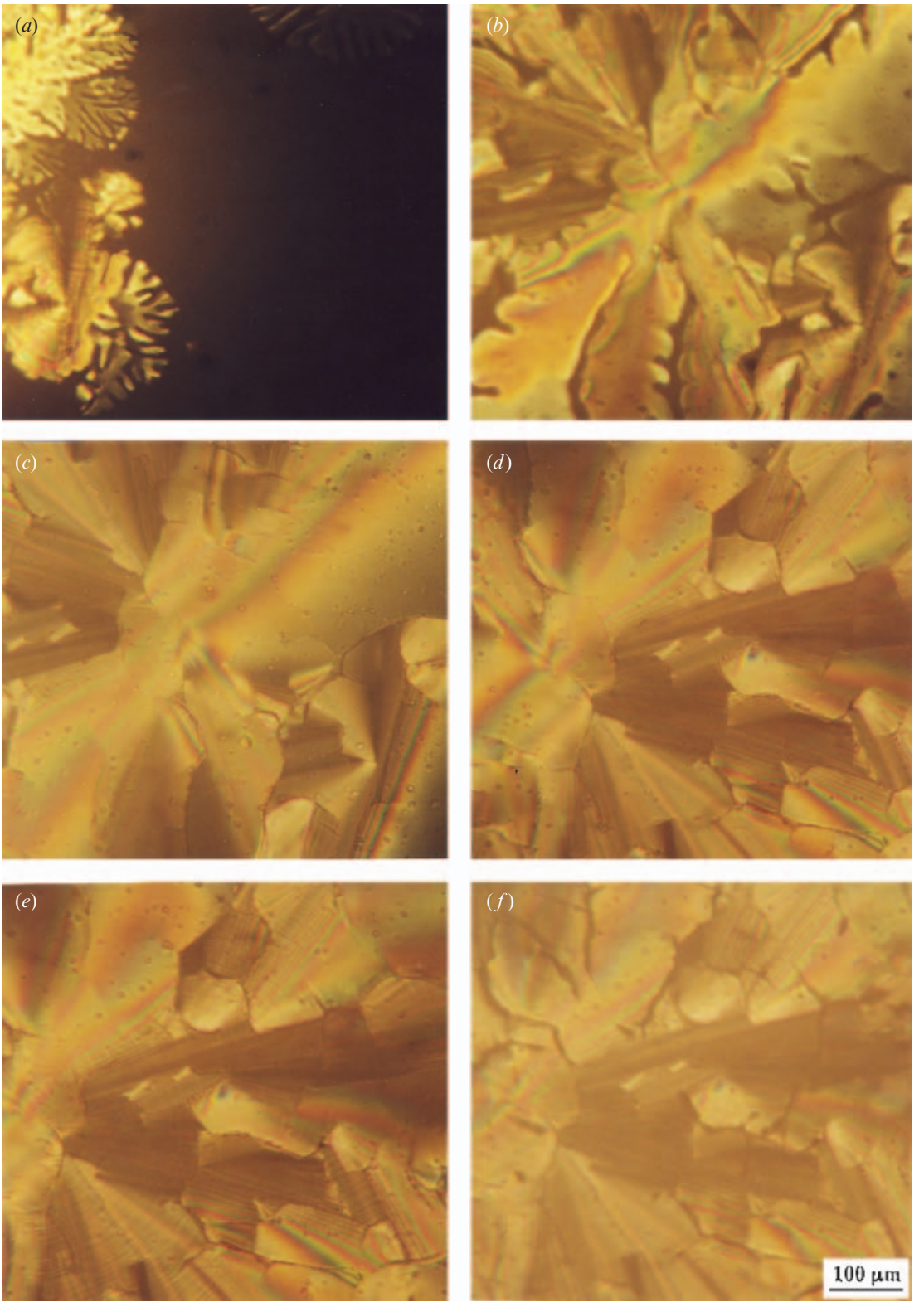

Figure 5. POM photographs of HOAQ(6) on cooling at atmospheric pressure: (*a*) formation of Col_h phase in the isotropic liquid at 105°C; (*b*) texture of the Col_h phase at 105°C after 5 min; (*c*) Col_h phase at 40°C; (*d*) Col_r phase at 10°C; (*e*) Col_r phase at 0°C; and (*f*) Cr_1 phase at −20°C.

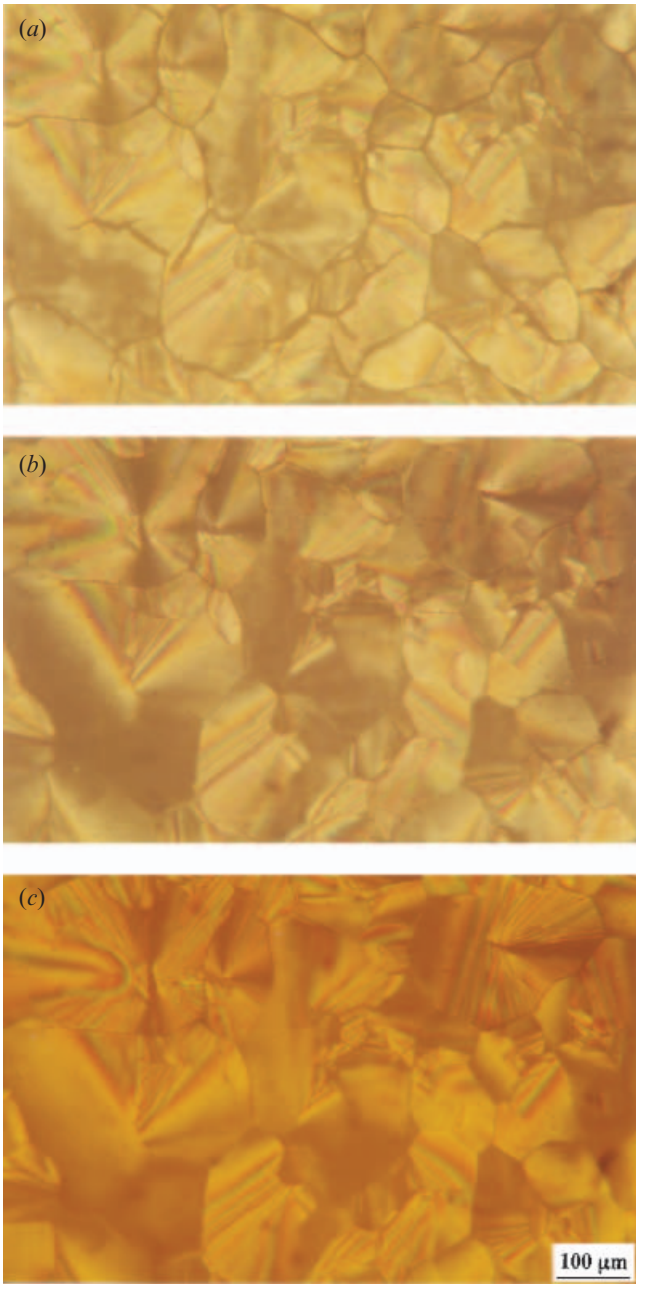

Figure 6. POM photographs of the textures of HOAQ(8) on heating: (*a*) Cr_1 at −15°C, (*b*) Col_r at 20°C, and (*c*) Col_h at 90°C.

domains in the Col_r phases at low temperatures, figures 5 (*d*) and 5 (*e*). The smaller mosaic texture did not change substantially during the Col_r–Cr transition, except for the change from distinct to indistinct domain boundaries. Figure 5 (*f*) shows the texture of the Cr_1 crystal at −20°C. The change in texture between the Cr_1 crystals and the isotropic liquid was completely reversible on subsequent thermal cycling. Figure 6 shows the mosaic textures of the Cr_1, Col_r and Col_h phases of HOAQ(8) at −15, 20 and 90°C on second heating process, respectively. HOAQ(8) exhibited the same changes in texture as seen for HOAQ(6) during the thermal cycling, but it is noted that the size of the mosaic domains is remarkably smaller than those for HOAQ(6), as shown in figure 5. Figure 7 shows the mosaic textures of the Col_r and Col_h phases of HOAQ(9) observed at 20 and 90°C on the second heating, respectively. In HOAQ(9) the potato-chip-like mosaics overlapped with each other, appearing different from those of HOAQ(6) and HOAQ(8) with sharp shapes. In general, however, mosaic textures are the common morphologies for the Col_h and Col_r phases seen for the HOAQ(*n*) homologous series.

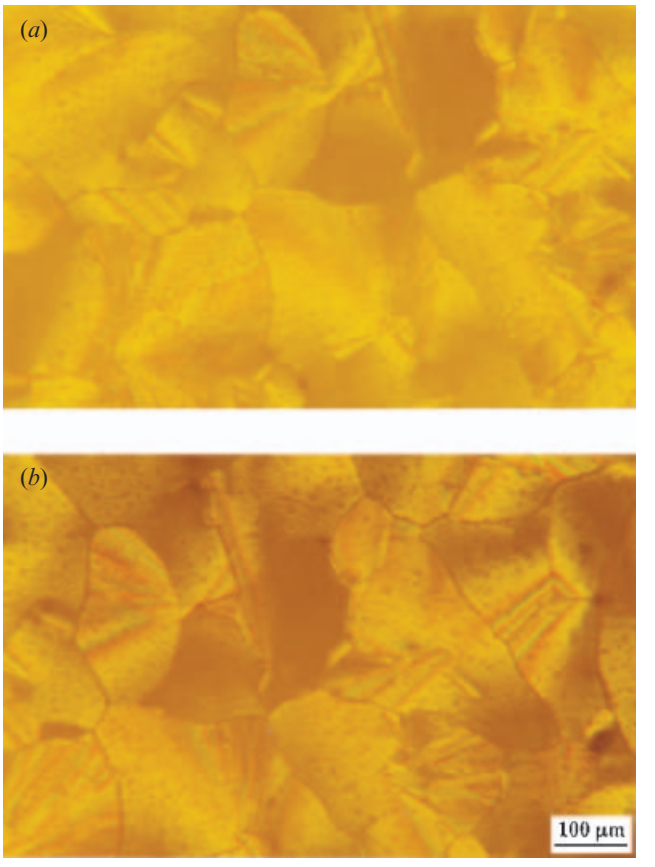

Figure 7. POM photographs of the textures of HOAQ(9) on heating: (*a*) Col_r phase at 20°C and (*b*) Col_h phase at 90°C.

Figure 8 shows the X-ray diffraction patterns of the Col_h phase of HOAQ(6), HOAQ(8) and HOAQ(9) on cooling from the isotropic liquid; they all show a spot-like Debye-Sherrer ring at $2\theta \cong 4°$–$5°$. The spot-like diffraction patterns correspond well to the mosaic textures of the Col_h and Col_r phases in figures 4–7. The *d*-spacings calculated from the reflection peaks of HOAQ(6), HOAQ(8) and HOAQ(9) are listed in table 2. The *d*-spacings of the (1 0 0) reflection at 80°C

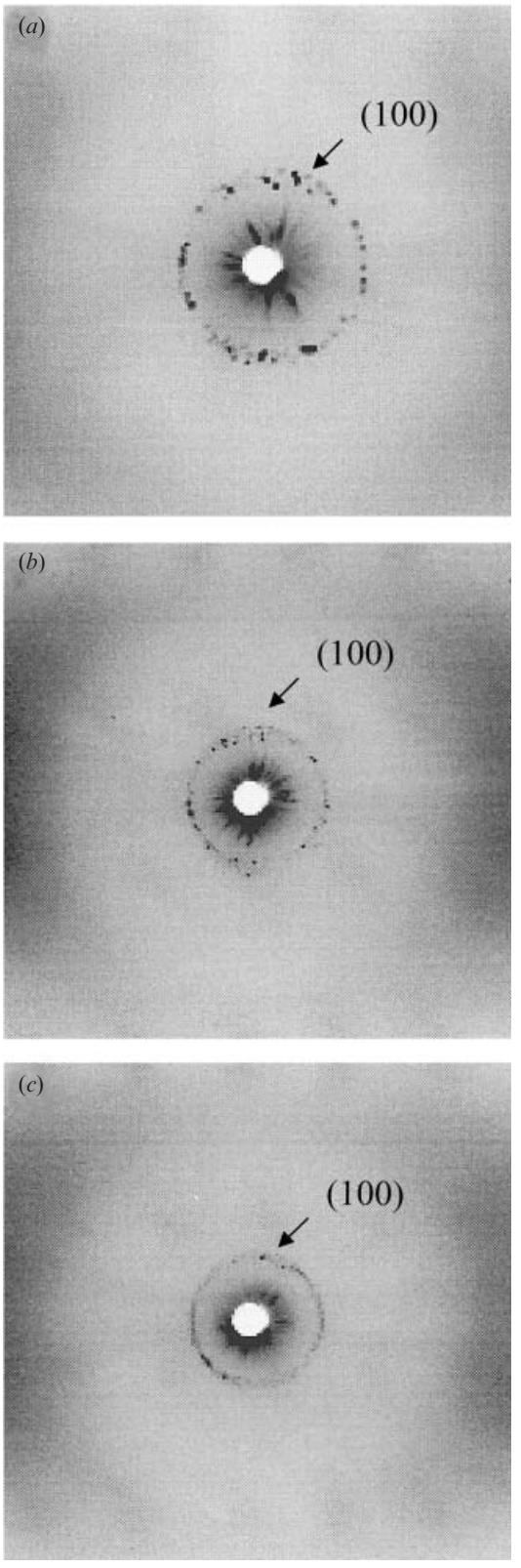

Figure 8. X-ray diffraction patterns of the Col_h phase for (*a*) HOAQ(6), (*b*) HOAQ(8) and (*c*) HOAQ(9) observed at 60, 60 and 40°C, respectively.

for the Col_h phase is estimated to be 1.78, 1.99, and 2.13 nm for HOAQ(6), HOAQ(8) and HOAQ(9), respectively. On the other hand, the Col_r phases of the three compounds show several strong reflections in the wide angle region along with the low angle reflections, indicating the existence of three-dimensional order in the Col_r phases. In HOAQ(8) the structure of the X phase is not clear at present as its diffraction pattern is substantially the same as that of the Col_r phase. The X-ray patterns of the Col_r phases closely resemble those of the Cr_1 phases.

3.2. *Thermal behaviour under pressure*

The thermal behaviour of the three HOAQ(*n*) samples was investigated under pressure to study the effect of pressure on the phase transitions of solution-grown and melt-cooled crystals for each compound. Figure 9 shows the DTA heating curves of the solution-grown sample of HOAQ(6) under various pressures. HOAQ(6) clearly shows the Cr_0–Col_r–Col_h–I phase sequence under pressures up to 100 MPa. The Cr_0–Col_r and Col_r–Col_h transition peaks approach each other with increasing pressure. Then the Col_r phase disappears under pressures above about 300 MPa, and the transition sequence changes to Cr_0–Col_h–I at higher pressures. At the same time the temperature region of the Col_h phase decreases with increasing pressure. The melt-cooled sample of HOAQ(6) exhibits the same transition behaviour as that of the solution-grown crystal shown in figure 9. The temperature region of the metastable Col_r phase is broader in the pressure region up to 100 MPa as the Cr_1–Col_r transition occurs at lower temperatures than the Cr_0–Col_r transition. Unfortunately the Col_r–Col_h transition on the second heating was not observed clearly under pressures above 200 MPa because the DTA signals at high pressures were too small to distinguish from the noise in the baselines. Figure 10 shows the *T*–*P* phase diagram of the two samples of HOAQ(6): the solid and broken lines are for the solution- and melt-crystallized samples, respectively, indicating the thermodynamically stable Cr_0 and metastable Cr_1 crystals. The *T*–*P* phase diagram reveals that the metastable Col_r phase has a broader temperature range than that of the stable Col_r phase. It is noted that the stable Col_r phase does not exist at high pressures above about 350 MPa. The Cr_0–Col_r transition point increases rapidly at low pressures and then changes gradually to a steady slope in the high pressure region, while the Col_h–I transition point increases linearly with a constant slope ($dT/dP = 0.025$°C/MPa), resulting in a rapid decrease in the temperature region of the mesophases consisting of the Col_r and Col_h phases.

Table 2. *d*-Spacings (nm) and $2\theta(^\circ)$ calculated from the X-ray reflections of the Cr_1, Cr_2, Col_r, and Col_h phases of the HOAQ(*n*) homologues.

HOAQ(6)	Solution-grown crystal	Melt-cooled crystal	Col_r phase	Col_h phase
	0°C	−30°C	10°C	80°C
	1.98 (4.45°)	1.92 (4.60°)	1.84 (4.80°)	1.78 (4.94°)
	1.34 (6.59°)	1.36 (6.50°)		
	0.97 (9.14°)	0.85 (10.34°)	1.06 (8.30°)	
	0.68 (12.96°)	0.61 (14.60°)	0.65 (13.58°)	
	0.56 (15.75°)	0.55 (15.95°)	0.57 (15.49°)	
	0.54 (16.40°)	0.53 (16.64°)	0.55 (15.94°)	
	0.45 (19.55°)	0.45 (19.79°)	0.44 (20.15°)	
	0.43 (20.49°)	0.43 (20.74°)	0.42 (20.90°)	
	0.42 (21.26°)		0.41 (21.50°)	
	0.38 (23.45°)	0.39 (22.55°)	0.39 (22.93°)	
	0.35 (25.04°)	0.35 (25.05°)		0.36 (24.35°)
	0.34 (26.01°)	0.34 (26.05°)	0.34 (25.95°)	
	0.32 (28.02°)	0.31 (28.15°)		
	0.28 (32.20°)			
	0.23 (38.05°)	0.23 (38.16°)	0.23 (37.97°)	
	0.21 (42.06°)	0.21 (42.26°)		
	0.20 (44.35°)	0.20 (44.44°)		
HOAQ(8)	Solution-grown crystal (Cr_2)	Melt-cooled crystal (Cr_0)	Col_r phase	Col_h phase
	25°C	−30°C	15°C	80°C
	1.59 (5.55°)	2.00 (4.40°)	1.99 (4.44°)	1.99 (4.44°)
		0.48 (18.35°)	0.49 (18.21°)	
	0.44 (19.95°)			
	0.42 (20.85°)			
	0.41 (21.50°)			
	0.39 (22.71°)			
		0.32 (27.88°)	0.32 (27.96°)	
	0.23 (37.95°)	0.24 (37.96°)	0.24 (38.00°)	0.24 (37.96°)
		0.21 (42.05°)	0.21 (42.09°)	
		0.20 (44.25°)	0.20 (44.27°)	
		0.19 (46.97°)	0.19 (47.12°)	
HOAQ(9)	Solution-grown crystal (Cr_2)	Melt-cooled crystal (Cr_0)	Col_r phase	Col_h phase
	25°C	−30°C	10°C	80°C
	2.03 (4.35°)	2.29 (3.85°)	2.32 (3.80°)	2.13 (4.15°)
	1.71 (5.15°)		1.85 (4.77°)	
	1.10 (8.03°)			1.21 (7.29°)
	0.93 (9.44°)			
	0.85 (10.34°)			
	0.68 (12.90°)			
	0.51 (17.34°)			
	0.47 (18.90°)	0.48 (18.40°)	0.48 (18.45°)	0.48 (18.41°)
	0.45 (19.45°)			
	0.43 (20.75°)			
	0.41 (21.75°)			
	0.39 (22.95°)	0.39 (22.63°)		
	0.37 (23.84°)			
	0.35 (25.45°)	0.35 (25.45°)	0.36 (24.70°)	0.36 (24.89°)
		0.27 (33.53°)		
		0.23 (38.14°)	0.23 (38.12°)	
		0.213 (42.29°)	0.214 (42.25°)	
		0.209 (43.25°)	0.209 (43.25°)	

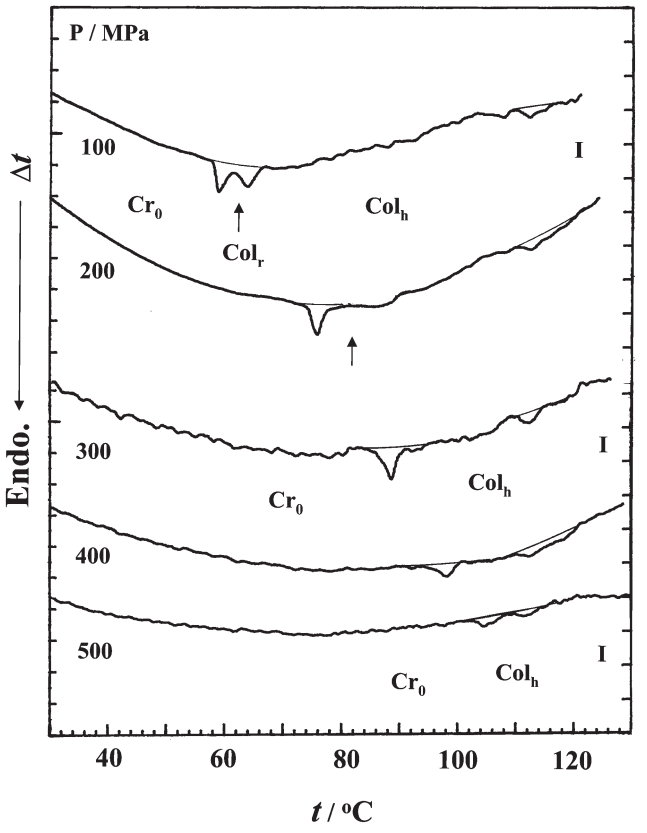

Figure 9. DTA heating curves of the solution-grown (Cr_0) sample of HOAQ(6) at various pressures. Heating rate: $5^{\circ}C\,min^{-1}$.

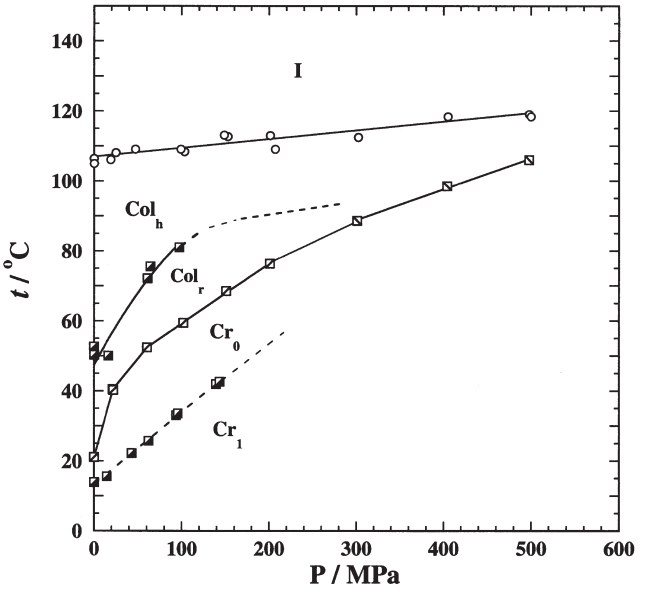

Figure 10. *T–P* phase diagrams of HOAQ(6). The solution-grown crystal (Cr_0) and melt-cooled crystal (Cr_1) are thermodynamically stable and metastable, respectively; otherwise differences between these are small. It is interesting to see that the reversible Cr_0–Col_r–Col_h–I transition sequence under atmospheric pressure is held at pressures up to about 200 MPa, while the Col_r phase disappears under pressures above 300 MPa.

The solution-crystallized sample of HOAQ(8) shows the Cr_{02}–Cr_{01}–Col_h–I phase sequence on first heating. Figure 11 shows the DTA heating curves of solution-grown crystals of HOAQ(8) at various pressures. The DTA melting peak of the Cr_0 crystal shows a large, broad transition peak with double peaks under pressures. It is noted here that the DTA heating curves on first heating exhibit the appearance of the stable Col_r phase under pressures above about 10 MPa, indicating the Cr_{02}–Cr_{01}–Col_r–Col_h–I phase sequence. Figure 12 shows the DTA heating curves of the solution-grown and melt-cooled samples of HOAQ(8) at 20 MPa for comparison. The solution-grown crystals exhibited the (Cr_{02}–Cr_{01})–Col_r transition with a large doublet peak at a high temperature, and the melt-cooled sample showed double melting peaks at very low temperatures and broad temperature regions of the Col_r and Col_h phases. Unfortunately the Col_r–Col_h transition was difficult to observe clearly under pressures because of the lack of sensitivity of the DTA signals. Figure 13 shows the *T–P* phase diagrams of the solution-grown and melt-cooled samples of HOAQ(8): the solid and broken lines indicate, respectively, the solution-grown crystals as a stable phase and the melt-cooled crystals as a metastable phase. The main difference between the Cr_0–Col_r and Cr_1–Col_r transition points is seen under all pressures: the relation of the melting points between the stable Cr_0 and the metastable Cr_1 crystals is apparent over the whole pressure region. We note that the Col_r phase appears as a stable phase in the pressure region between 10 and 350 MPa, and disappears at higher pressures. The temperature region of the Col_h phase decreases rapidly at pressures up to 100 MPa and then becomes constant (~10°C) at higher pressures. The solution-crystallized sample exhibits the phase sequence Cr_{02}–Cr_{01}–Col_h–I, both at atmospheric and high pressures above about 350 MPa, while the sample shows the phase sequence Cr_{02}–Cr_{01}–Col_r–Col_h–I in the intermediate pressure region. On the other hand, the melt-cooled sample shows the metastable Cr_1, X and Col_r phases under pressure, suggesting the phase sequence Cr_{12}–Cr_{11}–X–Col_r–Col_h–I. Unfortunately the X–Col_r and Col_r–Col_h transitions were not observed clearly under pressures above 100 MPa, because of the lack of sensitivity for the small signals.

As shown in figure 3, the DSC thermal behaviour of HOAQ(9) is very similar to that of HOAQ(8), except for the appearance of the unknown X phase. As already mentioned, the solution-grown samples of HOAQ(8)

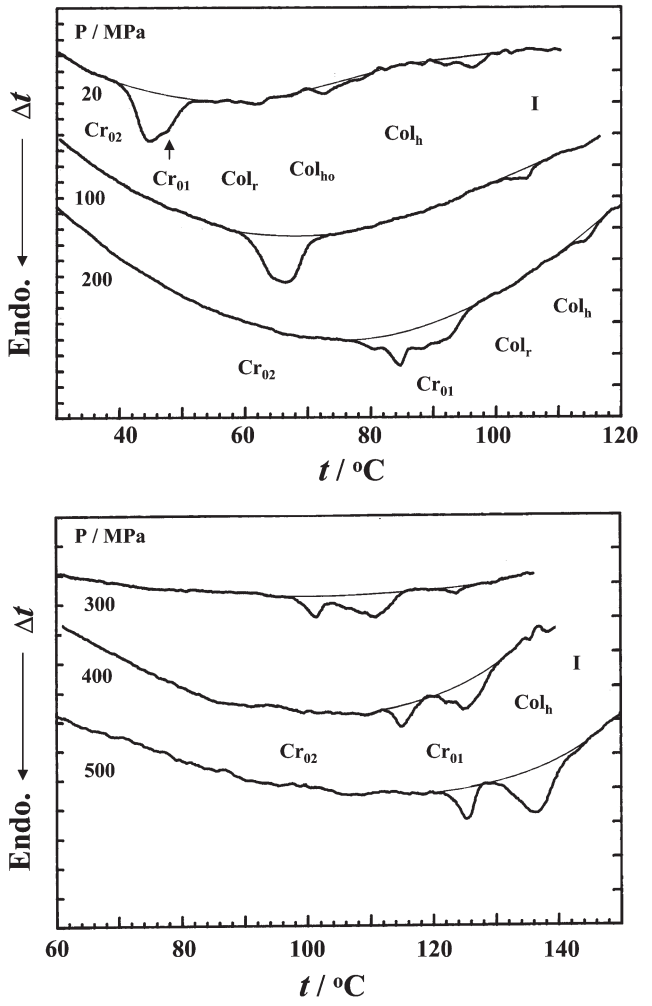

Figure 11. DTA heating curves of the solution-grown sample (Cr_0) of HOAQ(8) at various pressures.

and HOAQ(9) show several solid polymorphs, irrespective of the apparent single peak for the melting of HOAQ(9). The solution-grown sample of HOAQ(9) shows the stable Cr_0–Col_h–I phase sequence on first heating, while the melt-cooled sample shows reversibly the metastable Cr_1–Col_r–Col_h–I sequence. Figure 14 shows the DTA heating curves of solution-grown crystals of HOAQ(9) at various pressures. The Cr_0 crystals show a larger endothermic peak of melting than that of HOAQ(6). All the DTA heating curves under pressure show the melting and isotropization peaks at a higher temperature, indicating the phase sequence Cr_0–Col_h–I over the whole pressure range. Figure 15 shows the DTA heating curves of solution-grown and melt-cooled samples of HOAQ(9) at 100 MPa. The melt-cooled sample on the second heating run shows two additional peaks associated with the Cr_1–Col_r and Col_r–Col_h transitions, at lower temperatures than the Cr_0–Col_h transition temperature under pressures up to 300 MPa. Thus the Cr_1 and Col_r phases are metastable under all pressures. The metastable Col_r phase disappears at pressures above about 300 MPa, indicating that the metastable Col_r phase is unstable under high pressures. Figure 16 shows the *T*–*P* phase diagrams of the solution-grown (solid line) and melt-cooled (broken line) crystals of HOAQ(9). The metastable Col_r phase is located in the low pressure region below 300 MPa.

As listed in table 1, the apparent enthalpies of fusion for the Cr_0 crystals of HOAQ(8) and HOAQ(9) are extraordinarily large, i.e., 4–5 times larger than those for the melt-cooled Cr_1 crystals of the same compound. Since the melting of the solution-grown samples of HOAQ(8) and HOAQ(9) exhibit multiple peaks due to the inclusion of the solid–solid transitions and melting, it is difficult to estimate accurately the true enthalpy of fusion for the Cr_0–Col_h transition. Although the heat of fusion is not estimated for the Cr_0–Col_h transition for HOAQ(8) and HOAQ(9), it can be seen that the Cr_0 crystals of HOAQ(8) and HOAQ(9) are thermodynamically stable, because of their higher melting points than those of the melt-cooled Cr_1 crystals.

Based on the *T*–*P* phase diagrams, the transition curves for the stable phases of HOAQ(6), HOAQ(8) and HOAQ(9) can be expressed approximately as either first or second order polynomials in terms of pressure as:

Transition	HOAQ(6) (T/°C: peak temperature)
$Cr_0 \rightarrow Col_r$	$T/°C = 27.2 + 0.452\ (P/\mathrm{MPa}) - 1.080 \times 10^{-3}\ (P/\mathrm{MPa})^2$
$Cr_0 \rightarrow Col_h$	$T/°C = 62.2 + 0.088\ (P/\mathrm{MPa})$
$Col_r \rightarrow Col_h$	$T/°C = 47.4 + 0.469\ (P/\mathrm{MPa}) - 1.145 \times 10^{-3}\ (P/\mathrm{MPa})^2$
$Col_h \rightarrow I$	$T/°C = 107.0 + 0.025\ (P/\mathrm{MPa})$
	HOAQ(8)
$Cr_{02} \rightarrow Cr_{01}$	$T/°C = 39.2 + 0.258\ (P/\mathrm{MPa}) - 1.705 \times 10^{-4}\ (P/\mathrm{MPa})^2$
$Cr_{01} \rightarrow Col_r$	$T/°C = 41.9 + 0.275\ (P/\mathrm{MPa}) - 1.682 \times 10^{-4}\ (P/\mathrm{MPa})^2$
$Col_r \rightarrow Col_h$	$T/°C = 35.2 + 1.191\ (P/\mathrm{MPa}) - 6.710 \times 10^{-3}\ (P/\mathrm{MPa})^2$
$Col_h \rightarrow I$	$T/°C = 95.4 + 0.099\ (P/\mathrm{MPa})$
	HOAQ(9)
$Cr_0 \rightarrow Col_h$	$T/°C = 45.0 + 0.198\ (P/\mathrm{MPa}) - 1.050 \times 10^{-4}\ (P/\mathrm{MPa})^2$
$Col_h \rightarrow I$	$T/°C = 84.8 + 0.144\ (P/\mathrm{MPa})$.

The Col_h phases for HOAQ(6), HOAQ(8) and HOAQ(9) are thermodynamically stable, while the

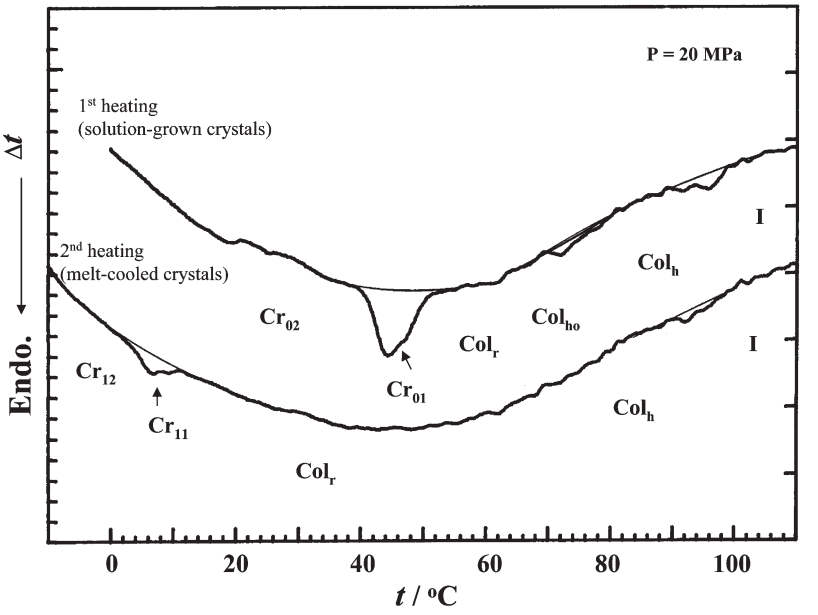

Figure 12. Comparison of the DTA heating curves of the solution-grown (Cr_0) and melt-cooled (Cr_1) samples of HOAQ(8) on the first and second heating processes at 20 MPa.

thermodynamic stability, either stable or metastable behaviour, of the rectangular columnar Col_r phase depends upon the temperature and pressure conditions.

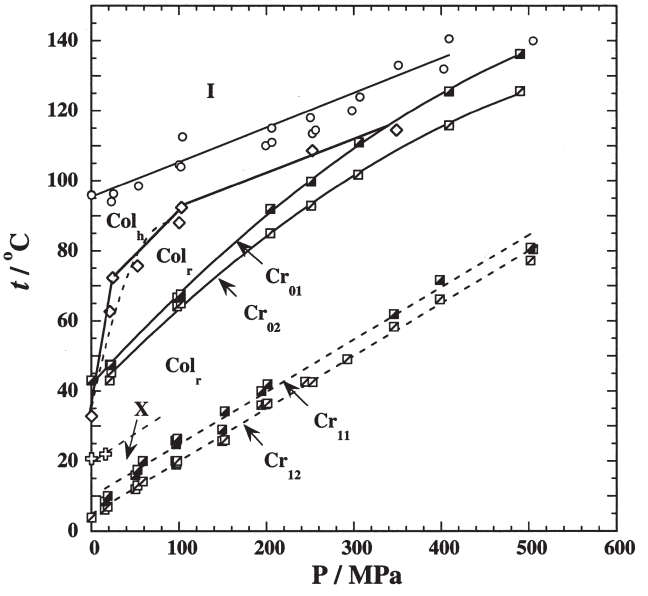

Figure 13. *T–P* phase diagrams of HOAQ(8). The Cr_0 and Cr_1 phases are, respectively, thermodynamically stable and metastable. The stable Cr_0–Col_{ho}–I phase sequence is observed under atmospheric pressure, but the Col_r phase appears stable between the Cr_0 and Col_h phases in the pressure range 10–400 MPa. However the Col_r phase disappears again at elevated pressures above 400 MPa. On the other hand, the metastable region of the Col_r phase is wide and the phase sequence Cr_1–Col_r–Col_h–I is observed under all pressures.

The Col_h–I transition point for the HOAQ(*n*) homologues is lowered with longer alkoxy groups. On the other hand, the linear slope of the Col_h–I transition becomes

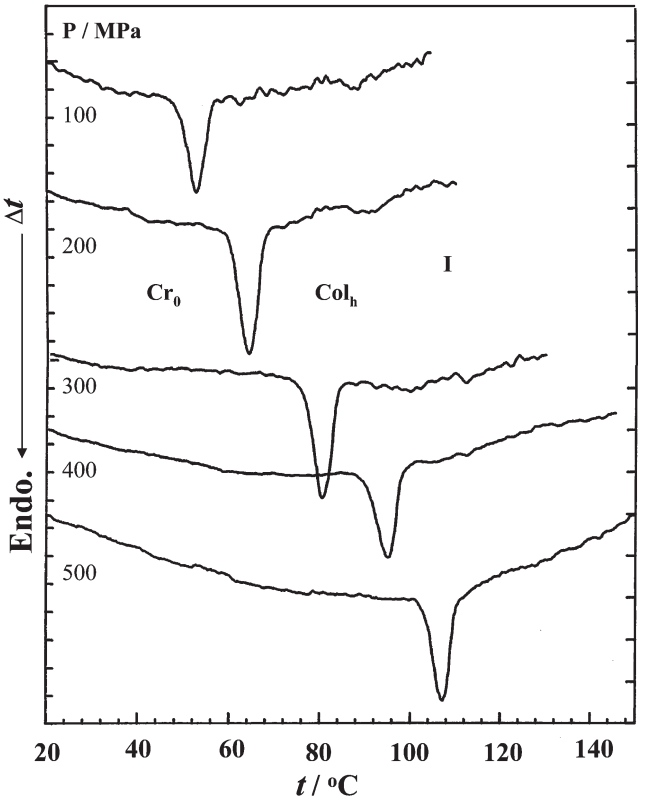

Figure 14. DTA heating curves of solution-grown crystals Cr_0 of HOAQ(9) at various pressures.

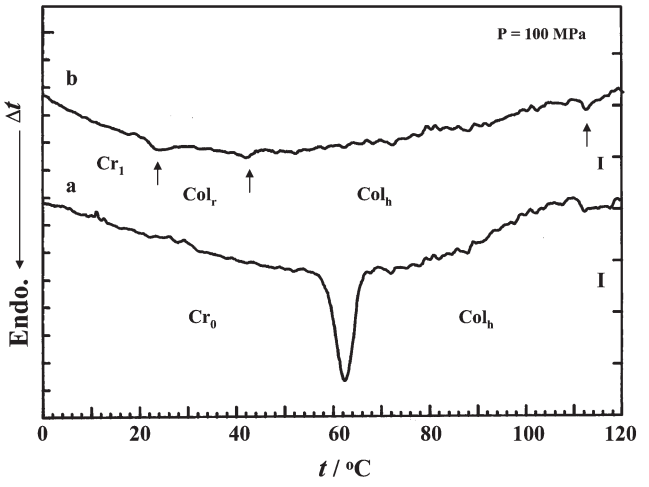

Figure 15. DTA heating curves of HOAQ(9) at 100 MPa.

larger on increasing the number of carbon atoms in the alkoxy chain from HOAQ(6) to HOAQ(9), while the slope of the Cr_0–Col_h transitions does not change significantly among the three compounds.

4. Conclusion

The transition behaviour of the 1,2,3,5,6,7-hexa-*n*-alkoxyanthraquinone HOAQ(*n*) homologues with alkoxy chains of n=6, 8 and 9, i.e. HOAQ(6), HOAQ(8) and HOAQ(9), was investigated under hydrostatic pressures up to 500 MPa using a high pressure DTA. The temperature vs. pressure phase diagrams of the solution-grown Cr_0 and melt-cooled Cr_1 crystals for the three compounds were constructed. The transition temperatures to the isotropic liquid phase decrease smoothly with increasing chain length of the alkoxy groups, indicating that the thermal stability of the Col_h phase decreases with the length of the flexible alkyl chains.

HOAQ(6) shows the reversible phase transition sequence Cr_0 (or Cr_1)–Col_r–Col_h–I at atmospheric pressure. The stable Col_r phase is observed at pressures up to about 300 MPa, while the metastable Col_r phase appears under all pressures. Pressure contributes to the change of the stable Col_r phase toward metastability. On the other hand, the solution-grown crystals of HOAQ(9) show the stable phase sequence $Cr_0 \rightarrow Col_h$–I without the stable Col_r phase under all pressures, while the melt-cooled sample exhibits the metastable Cr_1 and Col_r phases, showing the reversible transitions Cr_1–Col_r–Col_h–I under pressures up to 300 MPa. However the metastable Col_r phase disappears under pressures above 300 MPa, indicating the instability of the metastable Col_r phase at elevated pressures. HOAQ(8) exhibits a complex phase behaviour: the solution-grown

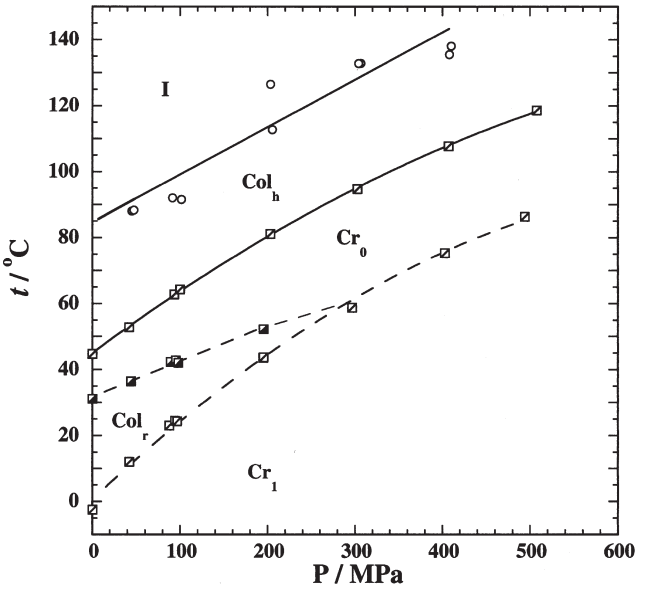

Figure 16. *T*–*P* phase diagram of HOAQ(9). The stable phase sequence Cr_0–Col_{ho}–I is observed under all pressures, while the metastable Col_r phase appears under pressures up to 300 MPa. The metastable Cr_1 crystals appear at all pressures.

sample shows the stable $Cr_0 \rightarrow Col_h$–I phase sequence at atmospheric pressure, but applying pressures above about 10 MPa on the Cr_0 crystals induces the stable Col_r phase between the Cr_0 and Col_h phases, leading to the $Cr_0 \rightarrow Col_r$–Col_h–I phase sequence; then the stable Col_r phase disappears again at elevated pressures above about 350 MPa. On the other hand, the melt-cooled sample shows reversibly the metastable Cr_1–X–Col_r–Col_h–I phase sequence under atmospheric pressure and hydrostatic pressures up to 100 MPa.

In general, the effect of pressure on the stability of the highly ordered rectangular columnar Col_r phase for the anthraquinone-based discotic mesogens is negative, because pressure contributes to the thermodynamic instability of the Col_r phase. An exception, however, is the positive effect of pressure on HOAQ(*n*) seen by the appearance of the stable Col_r phase of HOAQ(8) in the pressure region between about 10 and 350 MPa. The stable phase sequence Cr_{02}–Cr_{01}–Col_r–Col_h–I can be seen in the intermediate pressure region and then the pressure-induced Col_r phase also disappears under elevated pressures above 350 MPa, indicating a phase sequence Cr_{02}–Cr_{01}–Col_h–I. In the melt-cooled sample of HOAQ(8) the metastable Col_r and X phases appear with the metastable Cr_1 under all pressures, showing the phase sequence Cr_{12}–Cr_{11}–X–Col_r–Col_h–I.

The experimental observations in this study show that for the 1,2,3,5,6,7-hexa-*n*-alkoxyanthraquinone molecules with longer alkoxy chains the remarkable trend of the rectangular columnar phase decreasing in

phase stability on applying pressure is seen. The stable phase sequence of the HOAQ(*n*) compounds under pressure is Cr_0–(Col_r for HOAQ(6))–Col_h–I. On the other hand, the metastable Col_r phase is observed with the metastable Cr_1 crystals under all pressures. The Col_h phases are thermodynamically stable over the whole pressure region studied.

References

[1] S. Chandrasekhar, B.K. Sadashiva, K.A. Suresh. *Pramana*, **9**, 471 (1977).

[2] C. Destrade, H. Gasparoux, A. Babeau, H.T. Nguyen. *Mol. Cryst. liq. Cryst.*, **67**, 37 (1981).

[3] S. Chandrasekhar, B.K. Sadashiva, K.A. Suresh, N.V. Madhusudana, S. Kumar, R. Shashidhar, G. Venkatesh. *J. Phys. Paris*, **C3**, 120 (1979).

[4] C. Destrade, H.T. Nguyen, H. Gasparoux, J. Malthete, A.M. Levelut. *Mol. Cryst. liq. Cryst.*, **71**, 111 (1981).

[5] J. Billard, J.C. Dubois, C. Vaucher, A.M. Luvelut. *Mol. Cryst. Liq. Cryst.*, **66**, 115 (1981).

[6] S. Kumar. *Liq. Cryst.*, **31**, 1037 (2004).

[7] A. Queguiner, A. Zann, J.C. Dubois, J. Billard. In Proceedings of the International Conference on Liquid Crystals, Bangalore, S. Chandrasekhar (Ed.), p. 35, Heyden, London (1980).

[8] C. Carfagna, A. Roviello, A. Sirigu. *Mol. Cryst. liq. Cryst.*, **122**, 151 (1985).

[9] C. Carfagna, P. Iannelli, A. Roviello, A. Sirigu. *Liq. Cryst.*, **2**, 611 (1987).

[10] S. Kumar, J.I. Naidu, S.K. Varshney. *Liq. Cryst.*, **30**, 319 (2003).

[11] M. Werth, J. Leisen, C. Boeffel, R.Y. Dong, H.-W. Spiess. *J. Phys. II*, **3**, 53 (1993).

[12] H. Hollander, J. Hommels, K.O. Prins, H.-W. Spiess, M. Werth. *J. Phys. II*, **6**, 1727 (1996).

[13] B. Kohne, W. Poules, K. Praefcke. *Chem. Zig.*, **108**, 113 (1984).

[14] E.F. Gramsbergen, H.J. Hoving, W.H. de Jeu, K. Praefcke, B. Kohne. *Liq. Cryst.*, **1**, 397 (1986).

[15] E. Fontes, P.A. Heiney, W.H. de Jeu. *Phys. Rev. Lett.*, **61**, 1202 (1988).

[16] Y. Maeda, Y. Shimizu. *Liq. Cryst.*, **25**, 537 (1998).

[17] Y. Maeda, Y. Shimizu. *Liq. Cryst.*, **26**, 1067 (1999).

[18] Y. Maeda, D.S. Shankar Rao, S.K. Prasad, S. Chandrasekhar, S. Kumar. *Liq. Cryst.*, **28**, 1679 (2001).

[19] J.D. Adams, P. Schuhmacher, J. Simmerer, L. Haussling, K. Siemensmeyer, K.H. Etzbach, H. Ringsdorf, D. Haarer. *Nature*, **371**, 141 (1994).

[20] J.D. Adams, W. Römhildt, D. Haarer. *J. appl. Phys.*, **35**, 1826 (1996).

[21] J. Grimshaw, R.D. Haworth. *J. chem. Soc.* 4225 (1956).

[22] Y. Maeda, H. Kanetsuna, K. Nagata, K. Matsushige, T. Takemura. *J. polym. Sci. polym. phys. Ed.*, **19**, 1313 (1981); Y. Maeda. *Thermochim. Acta.*, **163**, 211 (1990).